Theory of the semiconductor photon echo

M. Lindberg, R. Binder, and S. W. Koch
Optical Sciences Center, University of Arizona, Tucson, Arizona 85721
and Department of Physics, University of Arizona, Tucson, Arizona 85721
(Received 26 August 1991)

The semiconductor Bloch equations are solved numerically for a two-pulse photon-echo configuration. The time-dependent diffracted signal is computed and the significance of many-body effects, carrier relaxation, and dephasing is investigated in detail. Assuming femtosecond-pulse excitation at various intensities and frequencies, distinctly different results are obtained if the exciton or the continuum electron-hole-pair states are excited. It is shown that pure exciton excitation produces a free-induction decay signal and no photon echo. An echo signal is obtained only if continuum states are excited either directly by choosing the central pulse frequencies appropriately or if the band-gap renormalization is sufficiently strong to shift continuum states into resonance. A continuous transition between free-induction decay and photon-echo signal is obtained with increasing excitation amplitude. A perturbative analytical analysis of the equations allows one to identify the role of the many-body effects in producing the different features.

PACS number(s): 42.50.Md, 42.65.Vh, 42.65.Hw

I. INTRODUCTION

In recent years it has been discovered that the optical response of direct-gap semiconductors shows some similarities to that of atomic systems if the time scales involved are shorter than the characteristic equilibrium times of the semiconductor electron-hole excitations. These conditions are best fulfilled for the case of pump-probe spectroscopy with picosecond or femtosecond pulses. The most studied example of such a "coherent" semiconductor response is the optical Stark effect, where a strong pump pulse excites that material energetically below the exciton resonance and the probe pulse monitors the transmission change at the exciton resonance [1–4].

Another well-known coherent phenomenon in atomic systems is the photon echo. Here, one uses short-pulse excitation of a system with a broad distribution of transitions, such as a cell of gas in thermal equilibrium where the velocity distribution of the gas atoms or molecules provides a continuum of Doppler-shifted transitions. Since the electronic single-particle states in semiconductors are energy bands, there is an intrinsic inhomogeneous distribution of the optical transitions involving electron-hole-pair excitation. This distribution of interband transition energies acts very much like the Doppler broadening in a gas. Therefore the photon echo is a very suitable technique to investigate similarities and differences between atomic and semiconductor systems.

Experimentally, photon-echo measurements are often used as a tool to determine the optical dephasing rate in atomic systems. This method has also been applied to semiconductors and information about the different carrier relaxation processes has been extracted [5–9]. Recently, evidence has been presented [9,10] that for a proper analysis of the photon echo in semiconductors the many-body effects in the system of electron-hole-pair excitations may lead to significant deviations from the atomic case.

In this paper, we investigate the temporal behavior of the photon-echo signal for a variety of different excitation conditions using the semiconductor Bloch equations for the case of a two-band semiconductor. These equations [11–15] not only describe the dynamical behavior of the light-induced polarization in semiconductors analogous to the well-known atomic two-level dynamics [16], but also include the Coulomb interaction and the excitation-induced many-body effects in the screened Hartree-Fock approximation. We treat the screening quasistatically, where the time dependence enters only parametrically through the distribution functions of the charge carriers. To extract the different scattering orders we use a spatial Fourier-series expansion for the equations and obtain an infinite set of equations, which we then truncate. For simplicity, scattering contributions due to a possible spatial dependence of the screening function are neglected. Optical dephasing and carrier collisions are described phenomenologically. We integrate the truncated set of equations numerically. Furthermore, we compare the numerical result with analytical evaluations using perturbation theory. Using a similar approach, Wegener *et al.* [17] recently investigated the time-integrated photon-echo signal for below-resonant excitation. In addition they studied phenomenological models with local-field effects to explain some of their numerical results.

In Sec. II of this paper we briefly review the semiconductor Bloch equations and discuss how scattering and screening can be included. A spatial Fourier analysis is performed in Sec. III and we derive the set of equations describing the photon-echo configuration and discuss how to solve them. Numerical results are presented in Sec. IV and some of the results are analyzed by analytical approximations in the Appendix. Conclusions are drawn in Sec. V.

II. SEMICONDUCTOR BLOCH EQUATIONS

The semiconductor Bloch equations for a parabolic, isotropic two-band semiconductor have been shown to be a very powerful model to study the optical properties of semiconductors [11–15,18]. The coherent part of the equations can be obtained easily by using the time-dependent Hartree-Fock approximation in the Hamiltonian equations of motion [14]. For a more complete description the scattering processes, dephasing, and Coulomb screening must also be included. The model, which we use to study the photon echo, is given by the semiconductor Bloch equations in the form

$$\frac{d}{dt}F_p^e=-iU_p^*P_p+iU_pP_p^*-\Gamma_p^e[F_p^2-f_P^e(\mu(t),T(t))]\ , \quad (1)$$

$$\frac{d}{dt}F_p^h=-iU_p^*P_p+iU_pP_p^*-\Gamma_p^h[F_p^h-f_p^h(\mu(t),T(t))]\ , \quad (2)$$

$$\frac{d}{dt}P_p=-(i\varepsilon_p+\gamma_p)P_p+iU_p(1-F_p^e-F_p^h)\ , \quad (3)$$

where $F_p^e=\langle a_p^\dagger a_p\rangle$ and $F_p^h=\langle b_p^\dagger b_p\rangle$ are the carrier populations and $P_p=\langle b_p a_p\rangle$ is the polarization for the momentum state p. Here $a_p^\dagger$, a_p, $b_p^\dagger$, and b_p are the creation and annihilation operators of conduction-band electrons and valence-band holes, respectively. The renormalized energy ε_p and the effective field U_p are functions of F and P:

$$\varepsilon_p=\varepsilon_p^0+\sum_{p'}(v_{p'}^s-v_{p'})-\sum_{p'}v_{p'}^s(F_{p+p'}^e+F_{p+p'}^h) \quad (4)$$

and

$$U_p=\frac{\mu_{cv}}{\hbar}E(R,t)+\sum_{p'}v_{p'}^sP_{p+p'}\ , \quad (5)$$

with ε_p^0 being the kinetic energy related to the reduced mass m_r of an electron-hole pair, μ_{cv} is the interband dipole matrix element, $v_p=4\pi e^2/p^2$ and v_p^s are the bare and screened Coulomb matrix elements, respectively, and we defined $e^2=e_0^2/\epsilon_0$, where e_0 is the elementary electron charge and ϵ_0 is the static background dielectric constant of the medium, respectively.

Since the photon echo is essentially a coherent phenomenon we have included relaxation and screening in a rather phenomenological way. The full scattering contributions in the semiconductor Bloch equations are very complicated and strongly nonlinear. In our phenomenological approximation the dephasing of the polarization is described with a rate term proportional to γ_p in Eq. (3). The population-scattering processes tend to distribute the electrons and holes in quasiequilibrium Fermi distributions within the respective bands. We use a linear approximation of the scattering integrals by including relaxation rates proportional to Γ_p^e and Γ_p^h in the population equations (1) and (2). The function $f_p(\mu(t),T(t))$ is the quasiequilibrium Fermi distribution with chemical potential $\mu(t)$ and carrier temperature $T(t)$. The chemical potential and the carrier temperature are fixed by the conservation of the total particle number and the total kinetic energy in the carrier-carrier scattering process. These quantities are determined such that $f_p(\mu(t),T(t))$ is that quasiequilibrium distribution function towards which the actual distribution function F_p would relax if after time t no other interactions were present.

The screening plays a quantitatively important role since it modifies the strength of the Coulomb interaction and thus of the nonlinearity. The screening in our treatment is taken into account quasistatically, i.e.,

$$v_p^s=v_p\left[1+\frac{\kappa^2}{p^2+\frac{C}{4}\kappa^2\left[\frac{\hbar p^2}{2m_r\omega_{\rm pl}}\right]^2}\right]^{-1}\ , \quad (6)$$

where κ is the inverse of the screening length, $\omega_{\rm pl}$ is the plasma frequency, and C is a fitting parameter set equal to 4 [19]. The inverse screening length is given by

$$\kappa^2=\frac{4\pi e^2}{\hbar^2\pi^2}\left[m_e\int_0^\infty dp\ F_p^e+m_h\int_0^\infty dp\ F_p^h\right] \quad (7)$$

and the plasma frequency by

$$\omega_{\rm pl}^2=\frac{4\pi e^2 n}{m_r}\ , \quad (8)$$

where n is the total carrier density. The screening of the Coulomb potential modifies the effective dipole energy U and gives rise to the screened-exchange and Coulomb-hole renormalization of the transition energy [19].

Equations (1)–(3) are derived assuming the system to be spatially homogeneous. We ignore coupling between the relative and center-of-mass motion and assume that the energy dispersion due to the center-of-mass motion can be neglected. This approximation, which is related to the Raman-Nath approximation [20], leaves the center-of-mass coordinate as a parameter R in the spatial dependence of the external-light field. We use this parameter later to perform a spatial Fourier transformation. The approximations made assume that the semiconductor is locally homogeneous on a spatial scale of the order of several Bohr radii, but its excitation varies on a scale of the order of the wavelength of the light. The light field in our case consists of two traveling waves propagating in different directions.

Since quite generally the optical response of a system depends strongly on its excitation spectrum it is of interest to review briefly the excitations contained in Eqs. (1)–(3) [19]. If the Coulomb potential is completely neglected, the equations are linear and the only coupling between different p states is due to the population-scattering term. In this case the equations essentially describe a set of two-level systems with a continuous distribution of excitation energies. The density of states has a lower limit, the band edge, and increases proportionally to the square root of the energy. Hence one of the basic elements of the semiconductor excitation spectrum is an energy continuum very similar to that of a gas. Another simple situation arises when we neglect the screening, by replacing v_p^s by v_p, as well as the so-called exchange terms, which are the nonlinear terms proportional to products of F and P in Eqs. (1)–(3). The equations then still contain a contribution of the Coulomb potential in

the form of an attractive potential in the polarization equation. For the case of an unexcited bulk semiconductor we can diagonalize the polarization equation using the hydrogen-atom states to obtain the linear semiconductor excitation spectrum consisting of the discrete exciton resonances and the interband excitation continuum [14].

III. THE SPATIAL FOURIER EXPANSION

We assume that the semiconductor sample is sufficiently thin so that we can neglect the reabsorption of the induced field. In this case we do not have to solve the detailed propagation problem and obtain the measured optical signal simply from the total induced-polarization density $P(t)$,

$$P(t)=\frac{1}{V}\sum_{p}P_{p} . \tag{9}$$

In photon-echo experiments the detector usually is in the far-field region. In order to compute the measured signal we therefore have to Fourier analyze the total polarization with respect to the spatial coordinate and select only those components which propagate in the direction of the detector. One of the standard photon-echo-measurement geometries consists of two laser beams propagating at a small angle with respect to each other and overlapping in the sample. A three-beam geometry [6–8] to produce stimulated photon echoes is also often used but in the present paper we concentrate on the two-beam case. The nonlinear interaction of the light beams with the material polarization produces a multitude of spatial scattering orders. These different scattering orders complicate the solution of the problem considerably.

In the rotating-wave approximation the total excitation field consists of two traveling waves given by

$$E(R,t)=E_1(t)e^{i\mathbf{k}_1\cdot\mathbf{R}}+E_2(t)e^{i\mathbf{k}_2\cdot\mathbf{R}} , \tag{10}$$

where both E_1 and E_2 have a dominant time dependence of the form $\exp(-i\omega t)$. We use the notation

$$\mathbf{k}_1=\mathbf{K}+\mathbf{k},\quad \mathbf{k}_2=\mathbf{K}-\mathbf{k} ,$$

and introduce spatial Fourier series expansions in the form

$$F_p=\sum_{n=-\infty}^{\infty}F_p^n e^{in\mathbf{k}\cdot\mathbf{R}} \tag{11}$$

and

$$P_p=\sum_{n=-\infty}^{\infty}P_p^n e^{i\mathbf{K}\cdot\mathbf{R}+in\mathbf{k}\cdot\mathbf{R}} . \tag{12}$$

Because F_p is real, we have the condition $F_p^n=(F_p^{-n})^*$. The equations of motion for the Fourier components take the form

$$i\frac{d}{dt}F_p^{en}=\frac{\mu_{cv}}{\hbar}[E_1(t)]^*P_p^{n+1}+\frac{\mu_{cv}}{\hbar}[E_2(t)]^*P_p^{n-1}-\frac{\mu_{cv}}{\hbar}E_1(t)(P_p^{-n+1})^*$$
$$-\frac{\mu_{cv}}{\hbar}E_2(t)(P_p^{-n-1})^*+\sum_{p'}v_{p'}\sum_{m=-\infty}^{\infty}[(P_{p+p'}^{m})^*P_p^{n+m}-P_{p+p'}^{n+m}(P_p^{m})^*]-i\Gamma_p^e(F_p^{en}-f_p^{en}) , \tag{13}$$

correspondingly for dF_p^{hn}/dt, and

$$i\frac{d}{dt}P_p^n=(\varepsilon_p^0-i\gamma_p)P_{p+p'}^n-\sum_{p'}v_{p'}P_{p+p'}^n-\frac{\mu_{cv}}{\hbar}E_1(t)(\delta_{n,1}-F_p^{e(n-1)}-F_p^{h(n-1)})-\frac{\mu_{cv}}{\hbar}E_2(t)(\delta_{n,-1}-F_p^{e(n+1)}-F_p^{h(n+1)})$$
$$-\sum_{p'}v_{p'}\sum_{m=-\infty}^{\infty}[(F_{p+p'}^{em}+F_{p+p'}^{hm})P_p^{n-m}-(F_p^{em}+F_p^{hm})P_{p+p''}^{n-m}] . \tag{14}$$

When the screening is included we choose not to Fourier analyze the screened potential even if it depends on the distribution functions and, hence, also in principle has a spatial dependence.

If the system initially has no excitation, we can see from the equations that only even harmonics ($n=2m$) of the population F and only odd harmonics ($n=2m+1$) of the polarization P appear. The odd Fourier components of F and the even components of P stay zero. If we neglect the higher scattering orders, the expansions for P_p and F_p take the form

$$P_p=P_p^1e^{i\mathbf{k}_1\cdot\mathbf{R}}+P_p^{-1}e^{i\mathbf{k}_2\cdot\mathbf{R}}$$
$$+P_p^3e^{i(2\mathbf{k}_1-\mathbf{k}_2)\cdot\mathbf{R}}+P_p^{-3}e^{i(2\mathbf{k}_2-\mathbf{k}_1)\cdot\mathbf{R}} , \tag{15}$$

$$F_p=F_p^0+F_p^2e^{i(\mathbf{k}_1-\mathbf{k}_2)\cdot\mathbf{R}}+(F_p^2)^*e^{i(\mathbf{k}_2-\mathbf{k}_1)\cdot\mathbf{R}} , \tag{16}$$

where the coefficients are independent of the spatial coordinates.

Equations (13) and (14) reveal an important difference between the many-body semiconductor system and a set of independent two-level systems. Our equations reduce to those of a two-level system if we put all Coulomb matrix elements equal to zero, or if we neglect the terms containing products of population and polarization Fourier components. For the case of two sequential pulses without temporal overlap and E_1 coming before E_2, the equations show that a set of independent two-level systems only produces the Fourier components F^0, $F^{\pm2}$, $P^{\pm1}$, P^{-3}, all other Fourier components remain zero. The signals are consequently propagating only in the directions $\mathbf{k}_1$, $\mathbf{k}_2$, and $2\mathbf{k}_2-\mathbf{k}_1$. However, when the bilinear terms are included, the system is a true interact-

ing many-body system. The bilinear terms mix the Fourier components in such a way that all spatial harmonics are created. For example, the signal in the direction $2\mathbf{k}_1-\mathbf{k}_2$ would then be completely given by the exchange effects and the measurement of this signal allows a direct estimate of the magnitude of these effects.

In practical calculations the set of equations is truncated in some finite order by neglecting all Fourier components of order higher than a chosen number. Note that this truncation is not equivalent to ordinary perturbation theory since it takes a part of the field effects up to infinite order. We solve the truncated equations numerically as discussed in Ref. [18].

The photon echo is seen in the direction $2\mathbf{k}_2-\mathbf{k}_1$ (corresponding to the Fourier component P_p^{-3}) if the pulse $E_1(t)$ hits the sample before the pulse $E_2(t)$ and in the direction $2\mathbf{k}_1-\mathbf{k}_2$ (corresponding to the Fourier component P_p^3) if the order of the pulses is reversed. Notice that reversing the time sequence of pulses with equal strengths is equivalent to taking a mirror image of the signal.

IV. RESULTS AND DISCUSSION

For the numerical evaluations we take the material parameters corresponding to CdSe, which has an exciton Rydberg energy $E_R \simeq 16$ meV and the masses are approximately $m_e \simeq 0.125 m_0$ and $m_h \simeq 0.431 m_0$. The scattering rates and the dephasing rate are taken to be phenomenological constants and for the present purposes we choose them all to be 5×10^{-3} fs^{-1}, which corresponds to $T_2=200$ fs. For this choice of parameters the $1s$ exciton is clearly resolved in the linear absorption spectrum. In this study we choose Gaussian excitation pulses with a temporal width of 100 fs [full width at half maximum (FWHM)]. Consequently, the pulses have a frequency bandwidth (FWHM) of the order of $2E_R$ in CdSe. If the central frequency of the pulses is chosen to be at the $1s$ exciton resonance, i.e., at E_g-E_R, the pulses barely have frequency components that are able to excite the continuum states.

One reason for the choice of CdSe rather than GaAs as our model substance in this paper is that we are interested in clearly distinguishing between the excitation of excitons and the continuum states. As discussed in Ref. [10], the smaller exciton binding energy in GaAs requires either large detuning or longer pulses to avoid direct excitation of continuum states.

We vary the amplitudes, i.e., the bare Rabi frequencies $\mu_{cv}E_1/\hbar$ and $\mu_{cv}E_2/\hbar$ for the pulses 1 and 2, respectively. In our notation the pulse $E_2(t)$ has its maximum always at $t=0$ so that the delay time τ is the time of the maximum of the pulse $E_1(t)$. Hence negative delay times imply that E_1 comes first, which is our standard situation.

To be able to distinguish the role of many-body effects in the photon echo for semiconductors it is instructive to recall the results for the case without many-body effects. The phenomenon of photon echo is based on a special preparation and a consequent free motion of an inhomogeneous set of oscillators [16]. For example, in a gas each atom or molecule is essentially independent and only the various Doppler shifts due to the velocity distribution cause an inhomogeneous distribution of the optical transitions. The free motion of the induced polarization for a single oscillator after a short pulse is given by

$$P(\varepsilon,t)=P(\varepsilon,0)e^{-i\varepsilon t-\gamma t}\ . \tag{17}$$

The total polarization is the sum over all excited osillators

$$P(t)=\int d\varepsilon\, D(\varepsilon)P(\varepsilon,0)e^{-i\varepsilon t}e^{-\gamma t}\ . \tag{18}$$

where $D(\varepsilon)$ is the distribution function of transition frequencies of the different oscillators. In the case of a semiconductor $\int d\varepsilon\, D(\varepsilon)P(\varepsilon,t)$ would correspond to $\sum_p P_p$. If the preparation of the system has been essentially independent of the frequency, such as in the case of a coherent broadband excitation, the total signal is just the Fourier transform of $D(\varepsilon)$. Consequently, the signal just decays monotonically after $t=0$.

However, other more interesting phenomena can be obtained if the excitation of the different oscillators has been phase dependent, which in the case of the photon echo is achieved by using the two consecutive pulses E_1 and E_2. The second pulse is strong enough that a nonlinear signal in the phase-conjugated direction can be created, starting from the conjugated-polarization component P^* created by the first pulse. The first pulse creates the polarization components essentially independently of the frequency. However, the free propagation during the time between the pulses causes energy-dependent phase changes. Assuming that the first pulse excites the sample at time $-|\tau|$, the polarization components traveling in the direction of the first pulse, just before the second pulse arrives at $t=0$, is given by

$$P^1(\varepsilon,t)\propto e^{-i\varepsilon(t+\tau)-\gamma(t+\tau)}\ . \tag{19}$$

Due to the nonlinear interaction the second pulse excites a polarization component proportional to $[P^1(\varepsilon,0)]^*$, which propagates in the direction $2\mathbf{k}_2-\mathbf{k}_1$. This component then acts as the initial value for integration of the photon-echo signal for later times. The signal is given as

$$\begin{aligned} P^{-3}(t)&\propto \int d\varepsilon\, D(\varepsilon)[P^1(\varepsilon,0)]^*e^{-i\varepsilon t}e^{-\gamma t}\\ &\propto \int d\varepsilon D(\varepsilon)e^{-i\varepsilon(t-\tau)}e^{(-\gamma(t+\tau)}\ , \end{aligned} \tag{20}$$

which is again the Fourier transform of the distribution function $D(\varepsilon)$. The phase-sensitive excitation has created a shift in the time argument. The maximum now occurs at the time $t=\tau$ after the second pulse and not at $t=0$ as in Eq. (18). This maximum in the signal is the photon echo and the value of the signal at the maximum proportional to $\exp(-2\gamma\tau)$, can be used to extract the dephasing rate γ. The integrated signal as a function of τ has a similar behavior. In order to obtain a clear photon echo, the distribution function $D(\varepsilon)$ must be sufficiently broad. However, if we assume in Eq. (20) that the distribution $D(\varepsilon)$ has only one frequency component, then the integral is reduced to one term and the signal decays monotonically starting from $t=0$ like

$$|P(t)|\propto e^{-\gamma(t+\tau)}\ , \tag{21}$$

and free-induction decay but no echo occurs.

These simple considerations let us expect that the photon echo in an ideal bulk semiconductor depends strongly on the excitation frequency and, since we assume pulsed excitation, the bandwidth of the pulse also becomes an important factor. In general we can say that if we excite resonantly at the exciton and the pulse bandwidth is less than one Rydberg energy, we would not expect to see a photon echo but only a single free-induction-decay type of signal. On the other hand, if the bandwidth is larger than the exciton Rydberg energy or if the center frequency of the pulse is in the band we would expect an echo. A mixed situation, in which both types of signals appear, is also possible.

In real semiconductors the concept of independent oscillators is lost and free motion after an initial excitation is very complicated due to the nonlinearity of the system. We will show that a very important factor is the excitation-dependent band-gap shift. This renormalization leads to a resonance condition which changes during the excitation due to the increase of the carrier density. Even if initially the excitation takes place at the exciton resonance energy, it is possible that during the excitation the band states may end up in resonance. Thus the strength of the excitation plays an important role as well.

First, we want to see what kind of signal the completely coherent system produces in the photon-echo direction for the case of low excitation. For this purpose we neglect completely the dephasing and the relaxation of the population but keep the quasistatic screening. We choose the delay time as $\tau=-300$ fs and the field strengths $\mu_{cv}E_1=0.01E_R$ and $\mu_{cv}E_2=0.1E_R$. In Fig. 1 we see the time dependence of the signal when the exciting fields are in exact resonance with the 1s exciton. The most important and somewhat surprising feature is that the signal seems to rise without limit. The rise is absent in atomic systems and is completely a consequence of the exchange contributions, as we discuss in the Appendix. Figure 2 shows that if we neglect the exchange contributions, the signal exhibits only a constant-level signal superimposed with the relatively small-amplitude oscillation due to the quantum beat between the 1s exciton and the 2s exciton. A comparison of the signal magnitudes in Figs. 1 and 2 shows that in the nonlinear system the contribution in Fig. 2 is completely masked by the much stronger rising signal. We do not expect the signal to increase up to infinity, but it will saturate at later times. There is no distinct peak to be seen in Fig. 1 which would correspond to the 300-fs delay time. Hence we cannot speak about a photon echo in this case, confirming our expectations that weak excitation of an isolated resonance does not produce a photon echo. However, the signal in Fig. 1 strongly deviates from the simple decaying signal, Eq. (21), which would result from a linear system such as uncoupled free excitons.

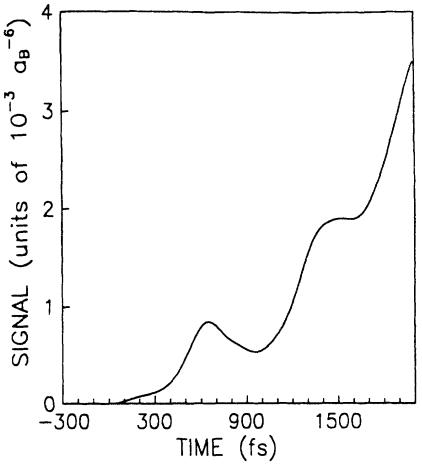

FIG. 1. Time-resolved signal in the direction $2\mathbf{k}_2-\mathbf{k}_1$ for excitation at the exciton resonance. The material parameters are chosen for CdSe, a_B is the exciton Bohr radius, E_R is the exciton binding energy, and the calculations were done for $T_2=\infty$ (no dephasing and no population relaxation), detuning $\delta=-1.0E_R$ (excitation at the exciton resonance), pulse width 100 fs (FWHM), delay time $\tau=-300$ fs (pulse E_1 comes 300 fs before pulse E_2), field strengths $\mu_{cv}E_1=0.01E_R$ and $\mu_{cv}E_2=0.1E_R$, where μ_{cv} is the interband dipole matrix element.

In Fig. 3 we assume excitation of the semiconductor at the band edge where a continuum of states is available. We keep all other parameters the same as in Fig. 1. Now the signal shows a clear echo which has its maximum about 300 fs after the second pulse. In Fig. 4 we demonstrate that a similar kind of signal is obtained also if the exchange effects are neglected. The photon echo occurs at the proper delay time and in addition we see now a small signal contribution caused by the beating between the 1s and 2s excitons, where the 2s exciton is weakly excited through the wing of the pulse spectrum. The comparison of the signal magnitudes shows that the exchange contributions strongly amplify the signal. In the Appendix we also discuss the amplification of the photon-echo signal in the nonlinear system when the continuum is excited.

In real semiconductors the dephasing and the scattering of the population play an important role. In fact, photon-echo experiments are often used to measure the

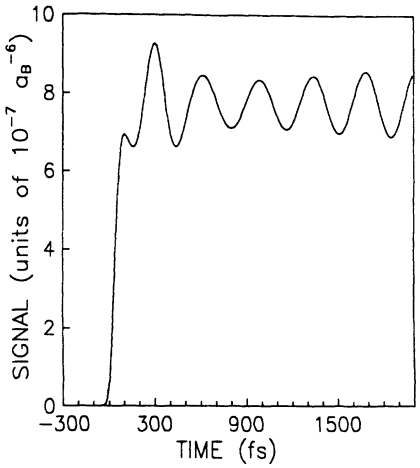

FIG. 2. Same as Fig. 1, but exchange terms are neglected.

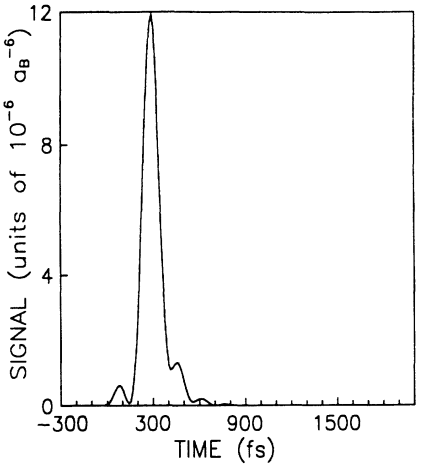

FIG. 3. Same as Fig. 1, but for excitation at the band edge, i.e., $\delta=0.0E_R$.

dephasing rates [6–9]. In what follows we therefore include the dephasing and the scattering. As a consequence the increase of the signal in Fig. 1 is expected to stop. In Fig. 5 we show the time dependence of the signal for various delay times from -400 to -150 fs for the case when the center frequency of the excitation is at the 1s-exciton resonance. The field strengths are again chosen to be $\mu_{cv}E_1=0.01E_R$ and $\mu_{cv}=0.1E_R$. The signal starts to rise when the second pulse hits the sample, but in contrast to Fig. 1 it has only a finite duration as a consequence of the dephasing. The time at which the signal peaks is not related to the delay time. In a measurement situation this kind of signal could, however, be easily confused with a real photon echo if by coincidence the delay time τ and the signal-peak time are not too different or if only time-integrated measurements are performed. The decrease of the signal magnitude with increasing delay time is due to the dephasing taking place between the pulses. The corresponding integrated signals as a function of delay time are shown in Fig. 6.

To see what happens when the continuum states are

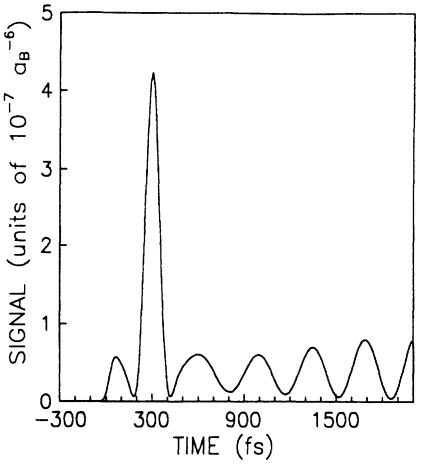

FIG. 4. Same as Fig. 3, but exchange terms are neglected.

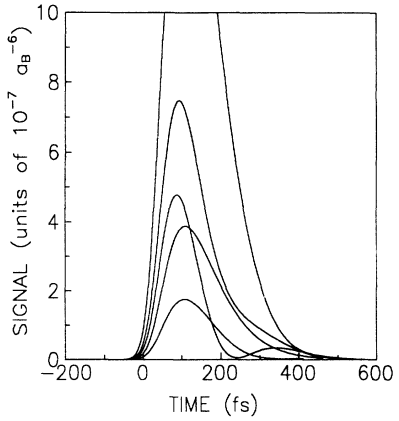

FIG. 5. Time-resolved signal in the direction $2\mathbf{k}_2-\mathbf{k}_1$ for excitation at the exciton resonance $\delta=-1.0E_R$, including dephasing and scattering, $T_2=200$ fs. The other parameters are the same as in Fig. 1, but the delay times τ are -150, -175, -200, -300, and -400 fs corresponding to decreasing signal maximum, respectively.

excited, we set the center-pulse frequency at the band edge. In Fig. 7 the signals with the same delay times and field strengths as in Fig. 5 are shown for delay times larger than the dephasing time. A clear echo feature can be seen essentially one delay time after the second pulse, as expected from the two-level-case analogy. The signal shows an additional peak centered around $t\simeq 50$ fs independently of the delay time. This component corresponds to the 1s exciton which is also excited due to the finite pulse bandwidth. The measurements of photon-echo signals of this kind have been reported in Ref. [21], however, for slightly different excitation and sample conditions. Figure 8 shows the integrated signal corresponding to Fig. 7 as a function of delay time. Fitting the curve formed by the maxima of the signals in Fig. 7 to the relation $|P|^2_{\max}\propto\exp(-4\tau/T_2)$ we regain the value used $T_2\simeq 200$ fs.

Even though the low-excitation results presented so far

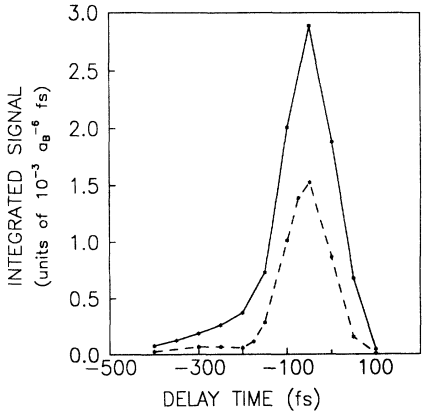

FIG. 6. Time-integrated signal (in units of 10^{-3} a_B^{-6} fs) in the direction $2\mathbf{k}_2-\mathbf{k}_1$ as a function of delay time for pulse strengths $\mu_{cv}E_1=0.01E_R$, $\mu_{cv}E_2=0.1$ (dashed line) and $0.5E_R$ (solid line). All other parameters are the same as in Fig. 5.

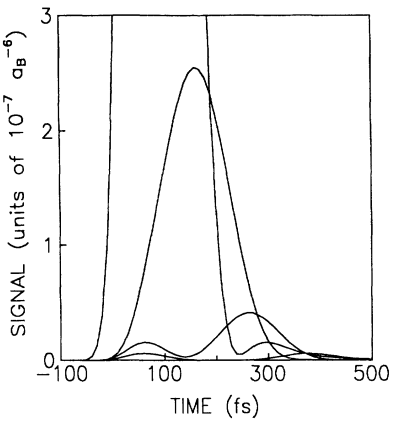

FIG. 7. Same as Fig. 5, but for excitation at the band edge. The delay times τ are -100, -200, -300, and -400 fs corresponding to decreasing signal maximum, respectively.

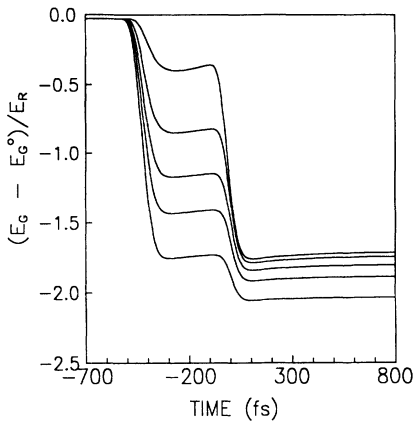

FIG. 9. Renormalized band edge as a function time. E_G^0 is the unrenormalized band gap. The delay time $\tau=-400$ fs and the different curves are for $\mu_{cv}E_1=0.01E_R$, $0.03E_R$, $0.05E_R$, $0.07E_R$, and $0.1E_R$, from top to bottom, respectively. All other parameters are the same as in Fig. 5.

exhibit some features which can be explained by considering the different exciton states as independent oscillators, similar to two-level atoms, our analysis shows that the many-body effects play a significant role in the dynamics. For example, if we neglect the many-body effects, the strengths of the signals are drastically modified. Furthermore, as discussed before, the increasing signal in Fig. 1 is a direct consequence of the exchange terms. Additionally, the band-gap renormalization can also be an important effect because it may completely modify the resonance conditions. To illustrate this feature, we plot in Fig. 9 the dependence of the band edge corresponding to Fig. 5 as the top curve. We see that the first pulse, which is very weak, leads to a shift of only about $0.3E_R$, whereas the second pulse causes a shift of the order of $2E_R$. In the case of such a large shift, a pulse which is originally centered at the 1s-exciton resonance causes direct excitation of the continuum states after the band gap has shifted by E_R. Nevertheless, this situation does not lead to a photon echo in Fig. 5, since the phase shifts necessary for the echo are produced in the time interval between the pulses [see Eqs. (19) and (20)] and during this time interval the band-edge shift in this case is still too small to allow significant continuum excitation by the first pulse.

However, for the same situation, only increasing the intensity of the first pulse, we should be able to shift and excite immediately part of the continuum so that the free propagation before the second pulse arrives is sufficient to cause the needed phase shifts for the photon echo. To demonstrate this effect we keep the center frequency of the pulses at the 1s-exciton resonance, fix the delay time at $\tau=-400$ fs, choose the strength of the second pulse as $\mu_{cv}E_2=0.1E_R$ and vary the strength of the first pulse. In Fig. 10 we show the resulting signals as a function of time for various field strengths of the first pulse. As expected, for low intensities the signal has a single peak near zero time, whereas for large intensities the peak of the signal is at 400 fs, which is the correct photon-echo time. The curves for intermediate intensities show the transition

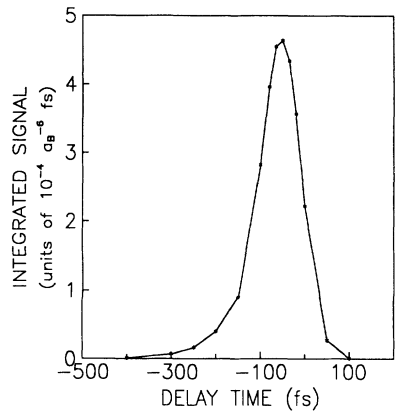

FIG. 8. Time-integrated signal corresponding to Fig. 7 as a function of delay time.

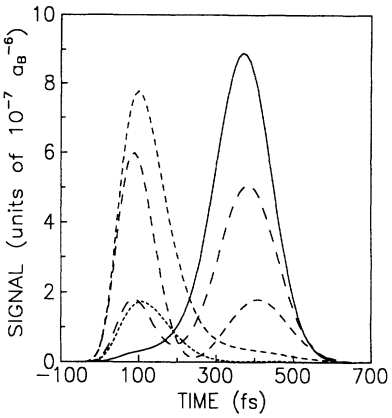

FIG. 10. Time-resolved signal in the direction $2\mathbf{k}_2-\mathbf{k}_1$ for increasing strength of the first pulse E_1. Excitation occurs at the exciton resonance $\delta=-1.0E_R$, $T_2=200$ fs; time delay $\tau=-400$ fs; pulse FWHM$=100$ fs; and $\mu_{cv}E_2=0.1E_R$. With increasing dash length, the curves are for $\mu_{cv}E_1=0.01E_R$, $0.03E_R$, $0.05E_R$, $0.07E_R$, and $0.1E_R$ (solid line).

from "free-induction decay" to "photon echo" taking place. A double peaked structure is seen to appear between the limiting cases. The band edges plotted in Fig. 9 correspond to the field strengths of Fig. 10 and we can see that for increasing $\mu_{cv}E_1$ the gap shift before the second pulse increases and exceeds E_R. Consequently, the band states are shifted into resonance with the field and the photon-echo signal develops.

To clarify further the different nature of the two peaks in the time-resolved signal in Fig. 10, we study their modifications caused by changing the dephasing rate. We choose pulses centered at the band edge, a delay time of -300 fs and the field strengths of $\mu_{cv}E_1=0.01E_R$ and $\mu_{cv}E_2=0.1E_R$, respectively. The resulting time-resolved signals are plotted in Fig. 11 for various T_2. The curve for $T_2=200$ fs shows two peaks, the first of which is caused by the weakly excited exciton and the second peak at $t=300$ fs is the real photon echo. The curves for $T_2=100$ and 50 fs show how the relative importance of the photon echo decreases with increasing dephasing rate, i.e., decreasing T_2. The overall signal level decreases also. These features are all related to the dephasing taking place between and after the exciting pulses. Both signal peaks experience the dephasing during the preparation period between the pulses, proportional to $\exp(-2\tau/T_2)$ causing the overall decrease of the signal with decreasing T_2. The first-signal contribution is generated essentially immediately after the second pulse because it is a pure free-induction decay signal. Therefore its peak value suffers no additional dephasing. The photon-echo peak, however, is a consequence of a constructive interference at time τ after the second pulse. During the time τ the individual oscillators have suffered a further decay proportional to $\exp(-2\tau/T_2)$ and consequently the photon-echo signal is reduced by this factor more than the induction decay signal. Therefore for small T_2 the free-induction decay component becomes the dominant feature of the overall signal.

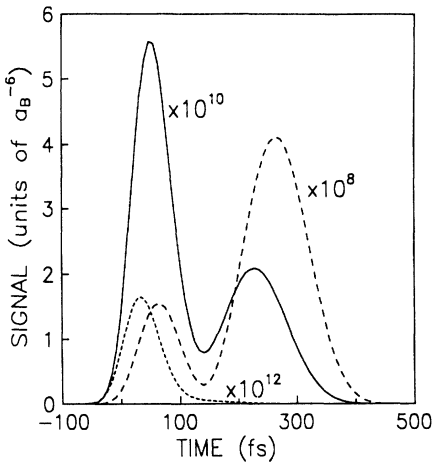

FIG. 11. Time-resolved signal for different dephasing times for excitation at the band edge, $\delta=0.0E_R$, $\tau=-300$ fs, $\mu_{cv}=0.01E_R$, and $\mu_{cv}=0.1E_R$. The dephasing times T_2 are 50 fs (short-dashed line), 100 fs (medium-dashed line), and 200 fs (solid line), respectively.

V. SUMMARY

In summary, we present a comprehensive numerical analysis of the semiconductor Bloch equations for conditions under which the photon echo in semiconductors can be investigated experimentally. For the material parameters of CdSe we show that the time-resolved signal exhibits features which can be clearly attributed to either exciton or continuum excitation. The exciton signal is characterized as free-induction decay which starts immediately after the excitation. For the artificial situation of vanishing dephasing this signal exhibits a predominantly linear increase which is caused by the exchange contributions in the electron-hole Fermi system. A true photon echo is obtained for resonant interband-excitation conditions. However, even for excitation into the exciton resonance we obtain a photon echo if the excitation intensity of the first pulse is sufficiently strong so that the band-gap renormalization shifts the continuum states into resonance during the presence of this pulse. With increasing excitation intensity we find a gradual transition from free-induction decay signal to the characteristic photon-echo scenario. Even though our numerical results are based on model equations for a two-band semiconductor with quasistatic screening and phenomenological inclusion of scattering and dephasing processes, we expect qualitatively similar behavior for real semiconductors.

ACKNOWLEDGMENTS

This work is supported by grants from the NSF, ARO, AFOSR, the Optical Circuitry Cooperative of the University of Arizona, and through a grant for CPU time at the Pittsburgh Supercomputer Center. R. B. acknowledges financial support by the DFG (Deutsche Forschungsgemeinschaft, Federal Republic of Germany).

APPENDIX

In this appendix we take an analytical approach to the semiconductor Bloch equations. The obvious way to simplify the equations is to use perturbation theory. We assume that both pulses are weak and solve the equations in first order in E_1 and second order in E_2 for the case when E_1 comes before E_2 assuming that the pulses have no temporal overlap. We do not include damping in these evaluations even if it would be straightforward. The equation we solve is given by

$$i\frac{d}{dt}P_p=\varepsilon_p P_p-U_p(1-2F_p)\ . \tag{A1}$$

To close the set of equations we use the constant of motion

$$(1-2F_p)^2+4|P_p|^2=1\ , \tag{A2}$$

which is valid if the relaxation is neglected. In the perturbative limit we can solve for F_p to obtain

$$F_p\simeq|P_p|^2+O(P^4)\ . \tag{A3}$$

Hence the equation of motion can be approximated by

$$i\frac{d}{dt}P_p \simeq \varepsilon_p^0 P_p - \sum_{p'} \nu_{p'} P_{p+p'} - 2\sum_{p'} \nu_{p'} |P_{p+p'}|^2 P_p + 2\sum_{p'} \nu_{p'} p_{p+p'} |P_p|^2 - \frac{\mu_{cv}}{\hbar} E(R,t)(1-2|P_p|^2) , \tag{A4}$$

with the initial condition $P_p(t=-\infty)=0$.

We now use the fact that the solution of the eigenvalue problem

$$\varepsilon_p^0 \phi_p^\lambda - \sum_{p'} \nu_{p'} \phi_{p+p'}^\lambda = \lambda \phi_p^\lambda \tag{A5}$$

is known [19]. The eigenfunctions form a complete orthonormal set of functions which we use to expand the polarization,

$$P^\lambda = \sum_p (\phi_p^\lambda)^* P_p , \tag{A6}$$

$$P_p = \sum_\lambda \phi_p^\lambda P^\lambda . \tag{A7}$$

Because we assumed no temporal overlap between the two pulses, we can choose a time t_0 such that the first pulse is gone and the second one has not yet come. For this time t_0 we can write the polarization in first order in E_1 in the form

$$P^\lambda(t_0) = i\sum_p (\phi_p^\lambda)^* e^{-i\lambda t_0} E_1(R,\lambda) \equiv i[\phi^\lambda(0)]^* e^{-i\lambda t_0} E_1(R,\lambda) , \tag{A8}$$

where $E_1(R,\lambda)$ is the Fourier transform of E_1 at frequency λ given by

$$E_1(R,\lambda) \equiv \int dt\, E_1(R,t) e^{i\lambda t} . \tag{A9}$$

The Fourier transform limits the range of the excitation within the bandwidth of the exciting pulse. We use this polarization as an initial condition when we integrate over the second pulse. The corrections to $P(t_0)$ are of third order in E_1. For times larger than t_0, the total polarization propagating in the direction $2\mathbf{k}_2-\mathbf{k}_1$ takes the form

$$\begin{aligned} P(t) \simeq & -2i\sum_p \sum_{\lambda,\lambda',\lambda''} \phi^\lambda(0)(\phi_p^\lambda)^* \phi^{\lambda'}(0)(\phi_p^{\lambda'})^* [\phi^{\lambda''}(0)]^* \phi_p^{\lambda''} [E_1(\lambda')]^* \\ & \times \int_{-\infty}^t dt' e^{-i\lambda(t-t')+i\lambda' t'} E_2(t') \int_{-\infty}^{t'} dt'' e^{-i\lambda''(t'-t'')} E_2(t'') \\ & -2\sum_{p,p'} \sum_{\lambda,\lambda',\lambda'',\lambda'''} \nu_{p-p'} \phi^\lambda(0)(\phi_p^\lambda)^* [\phi^{\lambda''}(0)]^* \phi_{p'}^{\lambda''} [\phi^{\lambda'''}(0)]^* \phi_p^{\lambda'''} [\phi^{\lambda'}(0)(\phi_{p'}^{\lambda'})^* - \phi^{\lambda'}(0)(\phi_p^{\lambda'})^*][E_1(\lambda')]^* \\ & \times \int_{-\infty}^t dt' e^{-i\lambda(t-t')+i\lambda' t'} \int_{-\infty}^{t'} dt'' e^{-i\lambda''(t'-t'')} E_2(t'') \int_{-\infty}^{t'} dt''' e^{-i\lambda'''(t'-t''')} E_2(t''') , \end{aligned} \tag{A10}$$

when only the first-order contributions in E_2 are taken into account. The first term in Eq. (A10), which does not vanish when the Coulomb matrix element ν_p is set to 0, describes the response of an inhomogeneous set of independent oscillators, which in this case are all the s excitons. The last term in Eq. (A10) is due to the exchange effects. Because of the multiple summations involved this expression is tedious to evaluate. We therefore make some rather drastic approximations in order to investigate the general features of the signal.

If the center frequency of the excitation is below the band gap, we expect that the bound excitons, which have a discrete spectrum, will become important. To concentrate on their effect we neglect all other excitons except the 1s exciton. In this case the signal is given by

$$\begin{aligned} P(t) \simeq & -2i[\phi^{\lambda_0}(0)]^3 \sum_p (\phi_p^{\lambda_0})^3 [E_1(\lambda_0)]^* \int_{-\infty}^t dt' e^{-i\lambda_0(t-t')} E_2(t') \int_{-\infty}^{t'} dt'' e^{i\lambda_0 t''} E_2(t'') \\ & -2[\phi^{\lambda_0}(0)]^4 \sum_{p,p'} \nu_{p-p'} [(\phi_{p'}^{\lambda_0})^2 (\phi_p^{\lambda_0})^2 - (\phi_p^{\lambda_0})^3 \phi_{p'}^{\lambda_0}][E_1(\lambda_0)]^* e^{-i\lambda_0 t} \int_{-\infty}^t dt' \left[\int_{-\infty}^{t'} dt'' e^{i\lambda_0 t''} E_2(t'') \right]^2 . \end{aligned} \tag{A11}$$

We are essentially interested in the long-time asymptotic behavior of the signal which we obtain from Eq. (A11) as

$$\begin{aligned} P(t) \simeq & -2i[\phi^{\lambda_0}(0)]^3 \sum_p (\phi_p^{\lambda_0})^3 [E_1(\lambda_0)]^* [E_2(\lambda_0)]^2 e^{-i\lambda_0 t} \\ & -2[\phi^{\lambda_0}(0)]^4 \sum_{p,p'} \nu_{p-p'} [(\phi_{p'}^{\lambda_0})^2 (\phi_p^{\lambda_0})^2 - (\phi_p^{\lambda_0})^3 \phi_{p'}^{\lambda_0}][E_1(\lambda_0)]^* [E_2(\lambda_0)]^2 e^{-i\lambda_0 t} t. \end{aligned} \tag{A12}$$

The first term, which is the familiar induction decay, gives only a constant signal, not an echo, as expected from an isolated oscillator. However, the exchange contributions produce a signal that monotonically increases with t. Figure 1 shows that this signal is seen in the numerical evaluations as the dominating contribution. As noted in Ref. [11], the multiplying coefficient of this term is the Heitler-London coefficient familiar from molecular physics, where exchange effects play an important role too. It is clear that physically this rising signal cannot be

correct for all times because of the conservation of the energy, indicating that our perturbation-theory approach is only valid at sufficiently short times.

The other limit is the case when the excitation frequency is well above the band gap in the interband absorption continuum. In this case we treat the Coulomb interaction perturbatively. We neglect the Coulomb interaction in the wave functions and keep it only in the exchange contributions as a multiplying matrix element in the sums, so that

$$\phi_p^\lambda \simeq \delta_{p\lambda}, \quad \phi^\lambda(0) \simeq 1 \ . \tag{A13}$$

The states are essentially free-particle states and consequently the eigenvalues λ are labeled by a momentumlike vector p_λ. The eigenvalues are given by

$$\lambda \simeq E_g + \frac{\hbar}{2m} p_\lambda^2 \ . \tag{A14}$$

The signal (A10) takes the form

$$P(t) \simeq -i \sum_\lambda [E_1(\lambda)]^* e^{-i\lambda t} \left[\int_{-\infty}^{t} dt' E_2(t') e^{i\lambda t'} \right]^2 - 2 \sum_{\lambda,\lambda'} \nu_{p_\lambda - p_{\lambda'}} [E_1(\lambda')]^* e^{-i\lambda t} \int_{-\infty}^{t} dt' (1 - e^{i(\lambda-\lambda')(t-t')}) \int_{-\infty}^{t'} dt'' E_2(t'') e^{i\lambda t''} \int_{-\infty}^{t'} dt''' E_2(t''') e^{i\lambda' t'''} \ . \tag{A15}$$

If we assume that the second pulse has the same lineshape function f and carrier frequency ω_0 as the first pulse, but is delayed by a time τ, we see that the echo signal from the first term is given by

$$P^1(t) \propto e^{-i\omega_0 t} \sum_\lambda [f(\lambda - \omega_0)]^3 e^{-i(\lambda-\omega_0)(t-2\tau)} \ . \tag{A16}$$

The signal is a kind of inverse Fourier transformation of the cube of the Fourier transformation of the pulse, but the maximum of the signal is shifted by 2τ from the peak of the first pulse. Thus the echo generally looks very much like the existing pulse itself but is broader in time.

To evaluate the exchange contributions we need the integral

$$G(t,t') = \sum_{p,p'} \nu_{p-p'} e^{i[\lambda(p)t + \lambda(p')t']} = \frac{e^2}{2\varepsilon} \frac{V}{(2\pi)^2} \left[\frac{2m}{\hbar} \right]^2 \frac{i}{\sqrt{|tt'|}} \frac{1}{t+t'} e^{iE_g(t+t')} F(t,t') , \tag{A17}$$

where $F(t,t')$ is defined by

$$F(t,t') = \begin{cases} 1 & \text{if } t \text{ and } t' \text{ have different signs} \\ i \, \mathrm{sgn}(t) & \text{if } t \text{ and } t' \text{ have same signs} \end{cases} \ . \tag{A18}$$

Since the integral form for arbitrary pulse shape does not reveal the behavior of the signal we assume for simplicity δ-function pulses. The signal contribution is then proportional to

$$-\frac{e^2}{2\varepsilon} \frac{V}{(2\pi)^2} \left[\frac{2m}{\hbar} \right]^2 e^{-iE_g(t-2\tau)} \Theta(t-\tau) \frac{i}{2\tau - t} \times \left[\sqrt{(t-\tau)/\tau} - \ln \left| \frac{t + 2\sqrt{\tau(t-\tau)}}{|t-2\tau|} \right| + i\pi \right] , \tag{A19}$$

where $\Theta(t)$ is the Heaviside step function. Equation (A19) shows that the signal diverges at $t = 2\tau$ as would also the first term given by Eq. (A16) if it had been calculated for δ-function pulses. The asymptotic behavior of the signal goes like $t^{-1/2}$ and the signal, hence, decays for large times in contrast to that of the exciton. Hence this signal contribution also shows an echolike feature which is supported by the numerical results in Sec. IV when the excitation takes place inside the band.

[1] A. Mysyrowicz, D. Hulin, A. Antonetti, A. Migus, W. T. Masselink, and H. Morkoc, Phys. Rev. Lett. **56**, 2748 (1986); A. Von Lehmen, D. S. Chemla, G. E. Zinker, and G. P. Heritage, Opt. Lett. **11**, 609 (1986).

[2] D. Fröhlich, R. Wille, W. Schlapp, and G. Weimann, Phys. Rev. Lett. **59**, 1748 (1987).

[3] N. Peyghambarian, S. W. Koch, M. Lindberg, B. Fluegel, and M. Joffre, Phys. Rev. Lett. **62**, 1185 (1989).

[4] W. Knox, J. B. Stark, D. S. Chemla, D. A. B. Miller, and S. Schmitt-Rink, Phys. Rev. Lett. **62**, 1189 (1989).

[5] A. M. Weiner, S. DeSilvestri, and E. P. Ippen, J. Opt. Soc. Am. B **2**, 654 (1985).

[6] L. Schultheis, J. Kuhl, A. Honold, and C. W. Tu, Phys. Rev. Lett. **57**, 1635 (1986); **57**, 1797 (1986).

[7] L. Schultheis, M. D. Sturge, and J. Hegarthy, Appl. Phys. Lett. **47**, 995 (1985).

[8] P. C. Becker, H. L. Fragnito, C. H. Brito Cruz, R. L. Fork, J. E. Cunningham, J. E. Henry, and C. V. Shank, Phys. Rev. Lett. **61**, 1647 (1988).

[9] K. Leo, M. Wegener, J. Shah, D. S. Chemla, E. O. Göbel, T. C. Damen, S. Schmitt-Rink, and W. Schäfer, Phys. Rev. Lett. **65**, 1340 (1990).

[10] S. W. Koch, R. Binder, and M. Lindberg, in *Quantum Electronics Laser Science, 1991*, Technical Digest Series (Optical Society of America, Washington, DC, 1991), paper QThA5, pp. 198 and 199.

[11] S. Schmitt-Rink and D. S. Chemla, Phys. Rev. Lett. **57**, 2752 (1986); S. Schmitt-Rink, D. S. Chemla, and H. Haug, Phys. Rev. B **37**, 941 (1988).

[12] W. Schäfer, K. H. Schuldt, and R. Binder, Phys. Status

Solidi B **150**, 407 (1988); W. Schäfer, Festkörperprobleme (Adv. Solid State Phys.) **28**, 63 (1988).

[13] I. Balslev, R. Zimmermann, and A. Stahl, Phys. Rev. B **40**, 4095 (1989).

[14] M. Lindberg and S. W. Koch, Phys. Rev. B **38**, 3342 (1988); S. W. Koch, N. Peyghambarian, and M. Lindberg, J. Phys. C **21**, 5229 (1988).

[15] R. Zimmermann and M. Hartmann, Phys. Status Solidi B **150**, 365 (1988).

[16] See, e.g., L. Allen and J. H. Eberly, *Optical Resonance and Two-Level Atoms* (Wiley, New York, 1975).

[17] M. Wegener, D. S. Chemla, S. Schmitt-Rink, and W. Schäfer, Phys. Rev. A **42**, 5675 (1990).

[18] R. Binder, S. W. Koch, M. Lindberg, N. Peyghambarian, and W. Schäfer, Phys. Rev. Lett. **65**, 899 (1990); R. Binder, S. W. Koch, M. Lindberg, W. Schäfer, and F. Jahnke, Phys. Rev. B **43**, 6520 (1991).

[19] See, e.g., the textbook, H. Haug and S. W. Koch, *Quantum Theory of the Optical and Electronic Properties of Semiconductors* (World Scientific, Singapore, 1990), and the references cited therein.

[20] A. M. Lazaruk, Opt. Spektrosk. **53**, 1059 (1982) [Opt. Spectrosc. **53**, 633 (1982)]; for a review see, e.g., H. J. Eichler, P. Günter, and D. W. Pohl, *Laser Induced Transient Gratings* (Springer, Berlin, 1986).

[21] M. D. Webb, S. T. Cundiff, and D. G. Steel, Phys. Rev. Lett. **66**, 934 (1991).